Available online at www.sciencedirect.com
ScienceDirect
Journal of Power Sources 173 (2007) 816–821
JOURNAL OF POWER SOURCES
www.elsevier.com/locate/jpowsour

Short communication

Effect of oxygen nonstoichiometry on photo-electrochemical properties of TiO_{2-x}

M. Radecka *, A. Trenczek-Zajac, K. Zakrzewska, M. Rekas

AGH University of Science and Technology, Al. Mickiewicza 30, 30-059 Krakow, Poland

Available online 21 May 2007

Abstract

Polycrystalline TiO_{2-x} pellets were equilibrated at 1220–1420 K in a flow of Ar + 7 vol.% H_2 gas mixture. The resulting deviation x from stoichiometric composition of titanium dioxide was determined gravimetrically. X-ray diffractometry revealed coexistence of rutile with Ti_nO_{2n-1} Magnéli phases. Optical reflectance and photocurrent spectroscopies served as experimental methods of the band gap determination. Polycrystalline TiO_{2-x} were used as photoanodes in a photoelectrochemical cell. The photocurrent response to the applied voltage was studied. It was found that TiO_{2-x} with x ca. 0.006 exhibited the best photoelectrochemical performance.

Keywords: Photoelectrochemical cell; Titanium dioxide; Nonstoichiometry; Magnéli phases; Photoelectrochemical properties; Quantum efficiency

1. Introduction

Nonstoichiometric rutile TiO_{2-x} seems to be an attractive material for many applications among which the photoanodes in photoelectrochemical cells for water decomposition are the most important from the point of view of the present work. Water decomposition into hydrogen and oxygen by means of light involves the use of a suitable semiconductor in which the absorption of light takes place.

Since the early work of Fujishima and Honda [1] demonstrating for the first time hydrogen generation by the photoelectrolysis in a photo-electrochemical cell, PEC, many semiconductors have been proposed for electrodes. However, the general conclusion is that titanium dioxide, due to its excellent chemical stability and the resistance to corrosion, is the most promising material for such a purpose [2].

Among many important requirements for the photoanode material, there are only two that are not fulfilled by stoichiometric TiO_2. The first one concerns the energy band gap, E_g, of about 3.0 eV, too high to provide a good match between the absorption spectrum of the photoelectrode with the solar spectrum. This mismatch results in the solar conversion efficiency, η, being too low for successful applications. The second factor that limits the solar conversion efficiency is a high electrical resistivity of stoichiometric TiO_2.

Considerable decrease in the electrical resistivity can be achieved in nonstoichiometric TiO_{2-x}. The easiest way to obtain the nonstoichiometric TiO_{2-x} with a controlled deviation from stoichiometry, x, is annealing under reducing atmosphere.

Much work has been devoted to the nonstoichiometric rutile TiO_{2-x}. In particular, the structural aspects such as formation of sub-oxides of titanium, Ti_nO_{2n-1} (Magnéli phases, $n = 1/x$), have been studied [3,4]. The nature of defects: oxygen vacancies, titanium interstitials and more complex structures such as Wadsley defects and crystallographic shear planes have been discussed [5]. As far as the electronic properties are concerned, the experimental evidence is scarce. It is known that the band gap energies of many sub-oxides of titanium Ti_nO_{2n-1} with low n (n below 9) are at least 10 times smaller than E_g of the stoichiometric TiO_2. Hence, the idea to search for a semiconductor belonging to a group of titanium sub-oxides, with a band gap corresponding to the light absorption over the visible range. On the other hand, the band gap of TiO_{2-x} with small x, i.e. close to the stoichiometric composition, has been found to increase with the increasing deviation from stoichiometry [6].

The effect of deviation from stoichiometry in TiO_{2-x} on the photoelectrochemical properties has been investigated to some extent.

Houlihan et al. [7] reported on the photoresponse of ceramic TiO_2 photoanodes reduced in CO/CO_2 atmospheres

* Corresponding author. Tel.: +48 126172526; fax: +48 126172493.
E-mail address: radecka@uci.agh.edu.pl (M. Radecka).

0378-7753/$ – see front matter © 2007 Elsevier B.V. All rights reserved.
doi:10.1016/j.jpowsour.2007.05.065

and attributed the observed changes in the spectral dependence of photocurrent to the different defect states. Subbarao et al. [8] undertook the systematic study of the influence of the non-stoichiometry in single crystals of TiO_{2-x} on their electrical resistivity and photoelectrical response.

Here, we report on the preliminary results on the effect of non-stoichiometry on the photoelectrochemical properties of TiO_{2-x} with the ultimate aim to use them as photoanodes in PEC. The optical properties in the vicinity of the fundamental absorption edge of nonstoichiometric TiO_{2-x} polycrystalline samples are presented as well. The problem of band gap energy determination of nonstoichiometric TiO_{2-x} is addressed by using two methods: all-optical spectrophotometry based on the diffuse reflection measurements and a spectral dependence of the photocurrent in the PEC. We expect that an increase in the electrical conductivity of TiO_{2-x} electrodes will result in a reduction of ohmic losses and may affect the recombination processes of non-equilibrium charge carriers. The lack of systematic studies of the effect of nonstoichiometry in the polycrystalline samples has been the motivation of this work. The aim of this paper is to determine the experimental conditions for reduction of stoichiometric, polycrystalline TiO_2 that could provide low electrical resistivity combined with an efficient photo-response, i.e. the conditions required for well-performing photoelectrode material.

2. Experimental

2.1. Sample preparation

Photoanode materials were prepared by mixing a fine-grain powder of anatase TiO_2 with a lubricant agent (weigh ratio 1:0.05) in an agate mortar. Pellets were formed by uniaxial pressing under 50 MPa followed by isostatic pressing under 250 MPa. Sintering was carried out at 1600 K for 5 h in air. Pellets were reduced in a mixture of 93% Ar + 7% H_2 under a flow of 60 sccm for 3.5 h at different temperatures. The deviation from stoichiometry, x, has been determined from a change in mass of pellets before and after reduction. It has been assumed that $x = 0$ before reduction.

2.2. XRD analysis

X-ray diffraction experiments were performed on Philips X'Pert Pro diffractometer with Cu Kα filtered radiation over 2θ range from 20° to 80°. Phase identification was carried out using the ICDD database.

2.3. Spectrophotometric studies

Fundamental optical transitions from the valence to the conduction band at room temperature were studied by optical methods. A Lambda 19 Perkin–Elmer double beam spectrophotometer equipped with a 150 mm integrating sphere was used to measure the spectral dependence of total and diffuse reflectance over a wide wavelength, λ, of range 250–2500 nm.

2.4. Photoelectrochemical studies

Photo-electrochemical cell (PEC) was constructed with the photoanode made of reduced TiO_2 and a Pt cathode. The pellets were placed in a special glass sample holder which protected the back-side of the sample from any contact with a liquid electrolyte. The shape of the semiconductor electrode exposed to the electrolyte was circular, with a surface area of about 1 cm^2. The PEC used in our experiments is described in detail elsewhere [9]. The electrolyte used for all measurements was a mixture of an universal Britton–Robinson buffer solution pH = 7.1 with 0.1 M KCl. Such a solution with at least 0.1 M ionic strength exhibits low electrical resistivity and the Helmholtz layer shows a high capacitance, which gives a negligible contribution to the total capacitance (this can be treated as the capacitors connected in series).

The photoelectrochemical experiments were carried out using a 450 W lamp simulating a solar spectrum. The optical system consisted of a light source, a grating monochromator (Triax 180 Jobin Yvon), an optical waveguide and a PEC equipped with a quartz window. Photocurrent was measured with a Keithley 6517A electrometer. Bias voltages were supplied from a Hewlett-Packard 34401A power supply. Data acquisition was controlled by a PC.

Taking into account the spectral dependence of the power delivered to the photoanode especially when one uses a light source and a monochromator, the output photocurrent data were normalized by dividing the photocurrent by the input light intensity.

3. Results and discussion

3.1. Nonstoichiometry and phase composition

Table 1 lists the results of phase composition, overall deviation from stoichiometry (expressed by x in TiO_{2-x} and by n in the formula Ti_nO_{2n-1}) and the electrical resistance of polycrystalline TiO_{2-x} samples obtained by reduction of stoichiometric

Table 1
The influence of the reduction temperature on the deviation from stoichiometry x phase composition and electrical resistivity of the polycrystalline TiO_{2-x}

No.	Reduction temperature (K)	Detected phases	Chemical formula	n in Ti_nO_{2n-1}	Resistivity (Ω)
1	As-prepared	TiO_2-rutile	TiO_2	∞	2.74×10^6
2	1220	TiO_2-rutile	$TiO_{1.994}$	167	465.6
3	1270	$TiO_2 + Ti_4O_7$	$TiO_{1.990}$	100	181.8
4	1340	$TiO_2 + Ti_4O_7$	$TiO_{1.969}$	32	175.1
5	1420	$Ti_9O_{17} + Ti_8O_{15}$	$TiO_{1.954}$	22	26.9

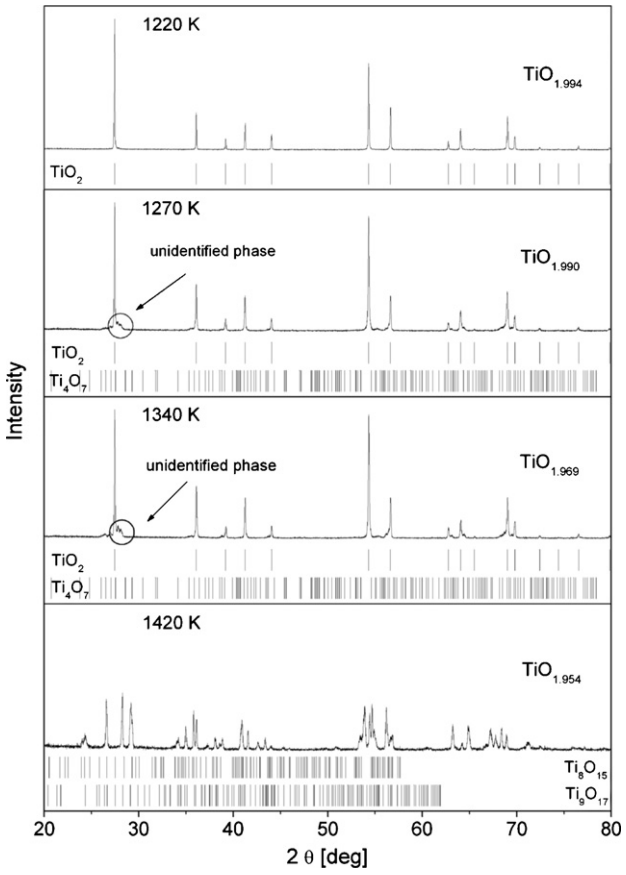

Fig. 1. X-ray diffraction patterns of the reduced samples and ASTM data of TiO_2 (rutile), Ti_4O_7, Ti_8O_{15} and Ti_9O_{17}.

(TiO_2) titanium dioxide at different temperatures. As clearly seen, the higher temperature under which the reduction is performed, the higher deviation from stoichiometry, x, is produced (lower n in the formula Ti_nO_{2n-1}). The reduction temperature affects the phase composition as well.

X-ray diffraction patterns of polycrystalline TiO_{2-x} samples after reduction are shown in Fig. 1. The samples reduced at the lowest temperature of 1220 K are homogenous. They crystallize in the rutile phase. Samples reduced at 1270 K contain the Ti_4O_7 phase along with the rutile phase of TiO_2. At the highest temperature of reduction (1420 K) the rutile is no longer formed. At least two phases Ti_8O_{15} and Ti_9O_{17} are identified in this case. However, there still remain some unidentified features in the X-ray diffraction patterns of samples reduced at the temperatures higher than 1270 K. This may be accounted for by formation of other Magnéli phases ($n > 10$).

A considerable effect of oxygen nonstoichiometry on the electrical resistivity is observed (Table 1).

3.2. Optical properties and the band gap

The width of the energy gap of semiconductors can be evaluated by means of several experimental techniques among which the spectrophotometry and photoelectrochemical methods play the most important role. All-optical methods such as spectrophotometry rely on the determination of the optical constants, i.e. the

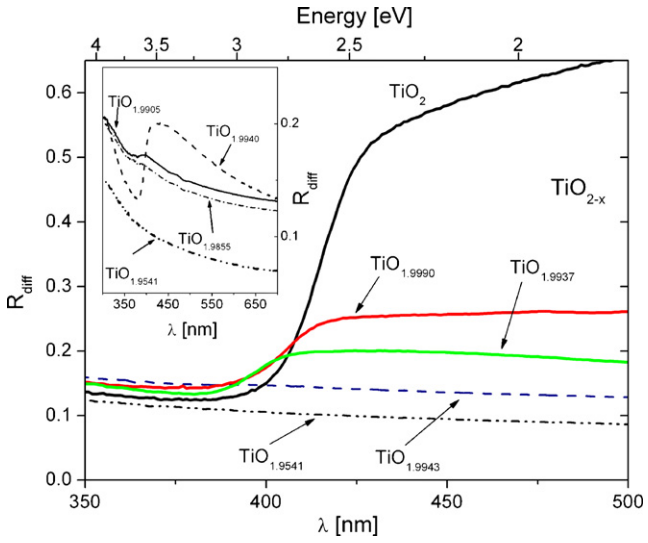

Fig. 2. Diffuse reflectance spectra for the reduced TiO_{2-x} samples and stoichiometric TiO_2.

refractive index and absorption coefficient from the measured spectral dependences of the transmittance and reflectance. In the case of ceramic samples, only the reflectance (total or diffuse) can be measured. The band gap energy, E_g, i.e. the energy of the fundamental optical transitions from the valence to the conduction band can be found [10,11] from the spectral dependence of the absorption coefficient.

The example of analysis of the fundamental transitions in polycrystalline TiO_2 samples based on the diffuse reflectance measured with the integrating sphere is given in Fig. 2. An abrupt increase in the reflectance coefficient, that occurs within a narrow range of wavelengths close to 400 nm is observed for stoichiometric TiO_2. This distinct edge of the optical reflectance may be correlated with the onset of the tail of the absorption curve and, in consequence, the optical band gap. The wavelength at the inflexion point corresponds to E_g. The plot of the differential reflectance $dR/d\lambda$ as a function of λ is presented of Fig. 3. The peaks at a certain wavelength are corresponding to the band gap of TiO_2.

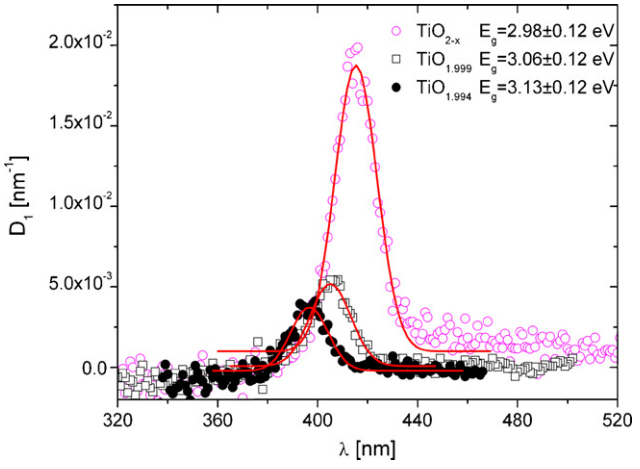

Fig. 3. $D_1 = dR/d\lambda$ vs. λ of the stoichiometric ($x = 0$) and reduced ($x = 0.001$ and $x = 0.006$) TiO_2 samples.

The total reflectance curve (Fig. 2) possesses a region of relatively constant reflectivity at shorter wavelengths ($\lambda < 400$ nm) due to the surface reflectivity of the material, since, provided the particles are completely absorbing, the absorption coefficient has little effect until the centre of the main absorption band is approached. At longer wavelengths ($\lambda > 450$ nm), the decreasing absorption coefficient results in the individual particles becoming relatively transparent, leading to multiple reflections and refractions in the bulk and a net increase in the diffuse reflectivity. The level at which the diffuse reflectance saturates is largely dependent on the value of the absorption coefficient, and when this is very low, the reflectivity approaches unity.

The diffuse reflectance of rutile is highly dependent on the precise stoichiometry [6]. The diffuse reflectance below the threshold for fundamental absorption (at wavelengths higher than 400 nm) decreases strongly with the increasing deviation from stoichiometry. Therefore, for highly reduced, nonstoichiometric samples this distinct linear region of the greatest slope in the reflectivity versus λ is no longer seen (Fig. 2). Additional states created by reduction allow for the absorption of light at the photon energies within the forbidden band gap. The energy of the band gap in such a case can be determined from the spectral dependence of the photocurrent.

3.3. Spectral dependence of photocurrent

Fig. 4 illustrates the normalized photocurrent density versus wavelength, λ. An abrupt change in the photocurrent over the wavelength range of 300–400 nm corresponds to the fundamental absorption edge in TiO_2. Over the visible region of the light spectrum, a local maximum in the photocurrent is seen at about 570–620 nm. Similar effect has been observed for thin film electrodes of TiO_2 and has been attributed to the surface defects of TiO_2 photoanodes [12]. Houlihan et al. [7] suggested that observed sub-bandgap light absorption (ca. 2.2 eV) could be accounted for by formation of titanium sub-oxides at the surface of the sample during reduction, but they failed to identify these phases. The band gap E_g can be determined from the analysis of the spectral dependence of the photocurrent or photoconductivity of the TiO_2 electrode in contact with a solution (both in dark and under illumination) [13]. The analysis is performed over the λ range of the fundamental absorption edge of TiO_2, i.e. 300–400 nm.

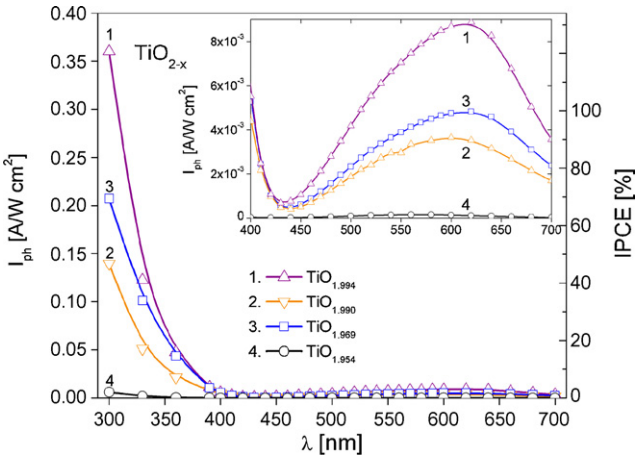

Fig. 4. Normalized photocurrent density, I_{ph}, (left axis) and IPCE efficiency (right axis) vs. wavelength, λ.

The method is based on the relationship between the quantum efficiency, η_q, of the photocurrent and photon energy, $h\nu$, [14,15]:

$$\eta_q = \frac{I_{ph}}{eJ_0} = 1 - \frac{\exp(-\alpha W)}{\alpha L + 1} \quad (1)$$

where I_{ph} is the photocurrent, e the elementary charge, J_0 the photon flux, α the optical absorption coefficient, L the minority carrier diffusion length and W is the depletion layer width, given by:

$$W = \left(\frac{2\varepsilon\varepsilon_0}{eN_d}\right)^{1/2} (V - V_{FB})^{1/2} \quad (2)$$

ε and ε_0 are dielectric constants of the oxide and vacuum, respectively, N_d the concentration of donors in the oxide, V and V_{FB} are the applied potential and the flat band potential, respectively. If the value of α is small enough so that:

$$\alpha W \ll 1 \quad \text{and} \quad \alpha L \ll 1 \quad (3)$$

the following approximations are valid:

$$\exp(-\alpha W) \approx 1 - \alpha W \quad (4)$$

and

$$\frac{1}{1 + \alpha L} \approx 1 - \alpha L \quad (5)$$

Inserting (4) and (5) into (1) we find:

$$\eta_q = \alpha(L + W) + (\alpha L)(\alpha W) \approx \alpha(L + W) \quad (6)$$

According to (3), the second order term of $(\alpha L)(\alpha W)$ in (6) may be neglected as compared with $\alpha(L + W)$.

In the vicinity of the absorption edge, the optical absorption coefficient, α, obeys the following relationship [10]:

$$\alpha = \frac{(h\nu - E_g)^\gamma}{h\nu} \quad (7)$$

where A is the absorption constant, $h\nu$ the photon energy, γ the parameter indicating the type of the fundamental optical transition ($\gamma = 1/2$ and $\gamma = 2$ for direct and indirect allowed transitions, respectively).

Combining Eqs. (6) and (7), we get:

$$(I_{Ph} h\nu)^{1/\gamma} = B(h\nu - E_g) \quad (8)$$

where

$$B = [eAJ_0(L + W)]^{1/\gamma} \quad (9)$$

Taking into account that parameter γ in Eq. (8) assumes value 2 for TiO_2 [16], the plots of $(I_{ph} h\nu)^{0.5}$ versus $h\nu$ have been drawn in Fig. 5 for three nonstoichiometric photoanodes. The band gap, E_g, is calculated from the intersection of the linear fit to the experimental data with the photon energy axis.

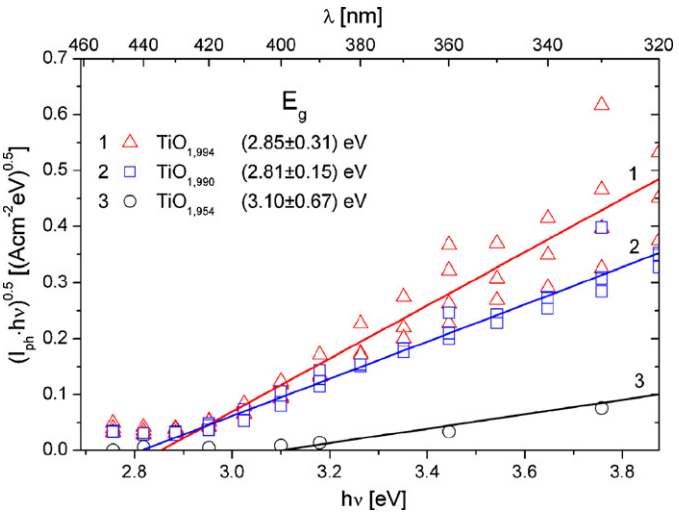

Fig. 5. $(I_{ph}h\nu)^{0.5}$ vs. $h\nu$ for: (1) $TiO_{1.994}$, (2) $TiO_{1.990}$ and (3) $TiO_{1.954}$.

Fig. 6 illustrates E_g versus oxygen nonstoichiometry, x, of the rutile phase. Solid circles correspond to spectrophotometric measurements; stars correspond to values determined from the photocurrent experiments (Eq. (8)), open circles were taken from Ref. [6]. As can be seen, all three sets of data show an increase in E_g with x within rutile phase stability. This effect can be easily explained by gradual filling up the narrow conduction band of the rutile phase, what is schematically shown in the inset of Fig. 6.

The observed differences between E_g derived from the optical and electrochemical experiments may result from either:

- Different electronic properties of near-surface layers in TiO_{2-x} where light absorption and creation of photocurrent occur.
- Different effects of extended defects or minority phases on both studied phenomena (optical absorption, creation of photocurrent).

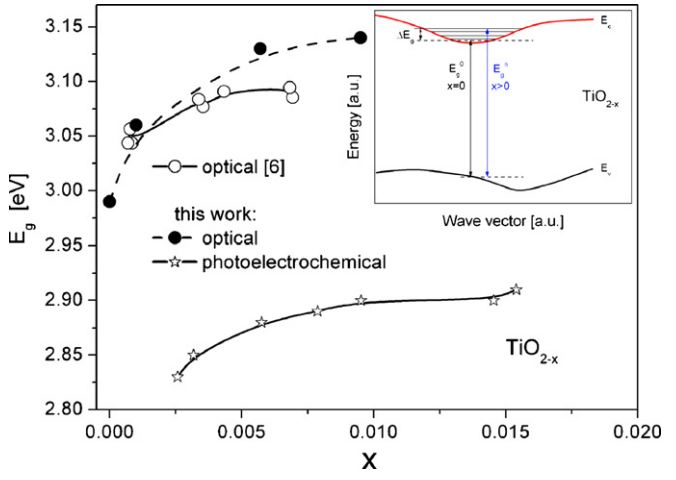

Fig. 6. Optical band gap, E_g, vs. x in TiO_{2-x}; solid circles—experimental points from optical measurements; open circles—results of Vratny and Micale [6]; stars—from photocurrent experiments. Inset shows schematical diagram explaining changes of E_g with nonstoichiometry.

3.4. Efficiency of the PEC

The photocurrent studies using monochromatic light allow us to determine the incident photon-to-current efficiency, IPCE:

$$\mathrm{IPCE} = \frac{hcJ_\lambda}{\lambda W_\lambda} \tag{10}$$

where h is the Planck's constant, c the velocity of light, J_λ the photocurrent density, λ the wavelength and W_λ is the power of the monochromatic light flux.

IPCE determines the number of electrons generated by light in the external circuit divided by the number of incident photons [16]. IPCE as a function of wavelength is presented in Fig. 4 (right axis). IPCE of the slightly reduced TiO_{2-x} ($2-x=1.994$) assumes the highest values, reaching ca. 120% in UV. The abrupt changes in IPCE with wavelength are observed for photons with energy $h\nu > E_g$. The local maximum close to 550–650 nm of IPCE is also observed. The IPCE above 100% may result from the departure of the studied system from a simple model that assumes creation of photon-pairs by excitation of electrons from the valence to conduction band, only. Apart from that, there are other contributions to the IPCE resulting from sub-band transitions [17] or photoreactions at the electrode/electrolyte interface [18,19].

Current density, I_{ph}, corresponding to darkness and to white light illumination is presented in Fig. 7 as a function of the electric bias, V_B, versus saturated calomel electrode, SCE.

The dark current assumes negligible values at positive potential. Exposure to light causes a considerable increase in the photocurrent. Anodic currents start at about −0.4 V. The threshold potential of the anodic current corresponds to the flat band potential, V_{FB}. The highest photocurrent is observed for $TiO_{1.994}$ photoanode. It is also shown that the electrodes with the highest nonstoichiometry: $TiO_{1.954}$ exhibit the lowest values of photocurrent. This may be correlated with the disappearance of rutile phase with the increasing deviation from stoichiometry. The presence of rutile seems to be a prerequi-

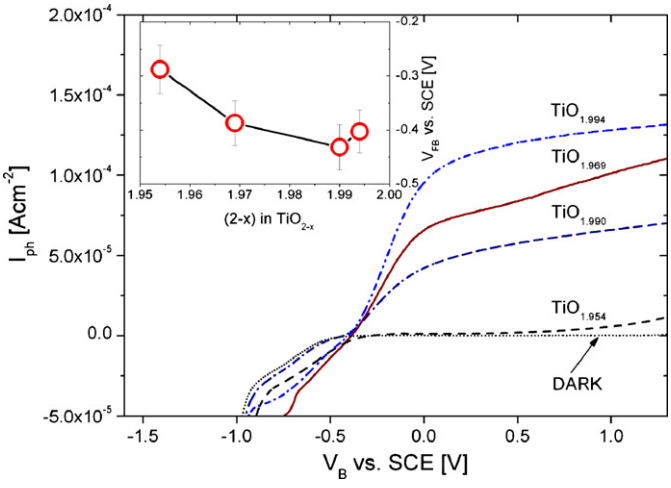

Fig. 7. Current–voltage characteristics, I_{ph}–V_B, for TiO_2 monitored in the dark and after illumination by white light. Inset—flat band potential, V_{FB}, vs. $(2-x)$ in TiO_2.

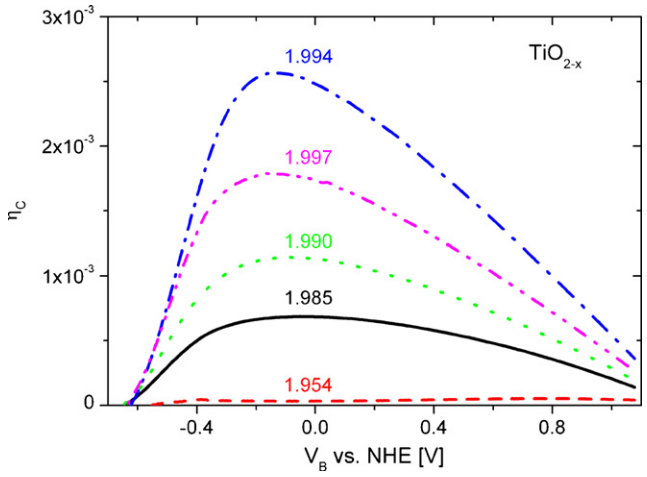

Fig. 8. Solar-to-hydrogen energy conversion efficiency, η_C, vs. electrical bias V_B.

site condition for good photoelectrochemical performance of the photoanode.

High deviation from stoichiometry has also a detrimental influence on the flat band potential. Negative value of the flat band potential required for photoelectrolysis of water becomes less negative with an increasing deviation from stoichiometry, x, of TiO_{2-x}.

Fig. 7 allows us to determine an overall efficiency of solar energy conversion, η_C [20] according to:

$$\eta_C = \frac{I_{ph}(1.23 - V_B)}{WS} \quad (11)$$

where W is the power of incident solar irradiation and S the surface of the irradiated electrode.

The highest efficiency for photons with energy lower than energy gap, E_g, is obtained for slightly reduced $TiO_{1.994}$ samples.

Fig. 8 shows η_C parameter as a function of a bias voltage. Samples that do not contain the rutile phase exhibit the lowest efficiency. The maximum value of η_C is observed at the electrical bias ca. 0 V. The photoelectrode of $TiO_{1.994}$ shows the highest efficiency at $V_B = -0.15$ V. As the ceramic, polycrystalline materials have been chosen for photoelectrodes in this paper it is worth noting that such electrodes will exhibit much lower efficiencies of solar energy conversion than their single-crystalline or thin film counterparts due to recombination processes occurring at surfaces, grain boundaries, etc. However, the choice of such materials can be justified by a low cost of photoanodes prepared by well-established methods and the ease with which large-area-electrodes are formed.

4. Conclusions

The effects of deviation from stoichiometry (expressed by either x or n in the formulas TiO_{2-x} and Ti_nO_{2n-1}, respectively) on structural, optical, electrical and photoelectrochemical properties were studied. It was found that the rutile phase existed for $0 \leq x \leq 0.006$, then some sub-oxides (mainly Ti_4O_7) appeared. When x surpassed 0.046, the rutile phase was no longer formed. The optical studies revealed the presence of the fundamental absorption edge for slightly reduced samples only. The energy band gap determined from both optical and photocurrent measurements increased with an increased deviation from stoichiometry, x. This phenomenon could be explained by a gradual filling up of a narrow conduction band in the rutile phase.

The detrimental effect of the reduction on the main photoelectrochemical parameters such as the flat band potential and the photoelectrochemical efficiencies (IPCE, η_C) was observed at the highest x values for which the rutile phase existed.

Acknowledgement

The financial support of the Polish Ministry of Education and Science under the project no. 3T08D 054 30 is greatly acknowledged

References

[1] A. Fujishima, K. Honda, Nature 238 (1972) 37–38.
[2] T. Bak, J. Nowotny, M. Rekas, C.C. Sorrell, Int. J. Hydrogen Energy 27 (2002) 19–26.
[3] S. Andersson, B. Collen, U. Kuylenstierna, A. Magneli, Acta Chem. Scand. 11 (1957) 1641–1652.
[4] S. Andersson, B. Collen, G. Kruuse, U. Kuylenstierna, A. Magneli, H. Pestmalis, S. Asbrink, Acta Chem. Scand. 11 (1957) 1653–1657.
[5] C.R.A. Catlow, R. James, Proc. Roy. Soc. Lond. A. Math. Phys. Sci. 384 (1982) 157–173.
[6] F. Vratny, F. Micale, Trans. Faraday Soc. 59 (1963) 2739–2749.
[7] J.F. Houlihan, D.B. Armitage, T. Hoovler, D. Bonaquist, D.P. Madacsi, L.N. Mulay, Mater. Res. Bull. 13 (1978) 1205–1212.
[8] S.N. Subbarao, Y.H. Yun, R. Kershaw, K. Dwinghta, A. Wold, Inorg. Chem. 18 (1979) 488–492.
[9] M. Radecka, K. Zakrzewska, M. Wierzbicka, A. Gorzkowska, S. Komornicki, Solid State Ionics 157 (2003) 379–386.
[10] J. Tauc, Mater. Res. Bull. 5 (1970) 721–729.
[11] G. Harbeke, in: F. Abelès (Ed.), Optical Properties of Solids, North-Holland Publishing Co., Amsterdam/London, 1972, pp. 23–92.
[12] A. Gorzkowska-Sobas, E. Kusior, M. Radecka, K. Zakrzewska, Appl. Surf. Sci. 600 (2006) 3964–3970.
[13] R.N. Pandey, K.S.C. Babu, O.N. Srivastava, Prog. Surf. Sci. 52 (1996) 125–192.
[14] W.W. Gärtner, Phys. Rev. 116 (1959) 84–87.
[15] M.A. Butler, J. Appl. Phys. 48 (1977) 1914–1920.
[16] J. Gerischer, in: B.O. Seraphin (Ed.), Solar Energy Conversion, Springer, Berlin, 1979, pp. 115–172.
[17] M.A. Butler, M. Abramowich, F. Decker, J.F. Juliao, J. Electrochem. Soc. 128 (1981) 200–2004.
[18] D. Laser, S. Gottesfeld, J. Electrochem. Soc. 126 (1979) 475–478.
[19] H. Morisaki, M. Hariya, K. Yazawa, Appl. Phys. Lett. 30 (1977) 7–9.
[20] B. Parkinson, Acc. Chem. Res. 17 (1984) 431–437.